

Anisotropic Growth and Formation Mechanism Investigation of 1D ZnO Nanorods in Spin-Coating Sol–Gel Process

Yijian Song¹, Maojun Zheng^{1,*}, Li Ma², and Wenzhong Shen¹

¹Laboratory of Condensed Matter Spectroscopy and Opto-Electronic Physics, Department of Physics, Shanghai Jiao Tong University, Shanghai, 200240, People's Republic of China

²School of Chemistry & Chemical Technology, Shanghai Jiao Tong University Shanghai, 200240, People's Republic of China

ZnO nanorods are fabricated on glass substrate by spin-coating sol–gel process using non-basic aged solution and annealing. Sample solutions reserved in room temperature for different time (one day, one month, two months and four months) are prepared for the experiment. The morphology study indicates that the aging time has direct influence on the final products. This is verified by the Transmission Electron Microscopy and Photon Correlation Spectroscopy study. Small crystalline nanoparticles would gradually nucleate and aggregate in the sol during the aging process. They act as nucleation site for the secondary crystal growth into nanorods during anneal. Both the size of crystalline particles in the sol and the size of nanorods will grow bigger as the aging time increases. The products' structure and optical property are further studied by X-ray diffraction spectroscopy, Photoluminescence and Raman spectroscopy. This work also helps to further clarify the formation mechanism of ZnO nanorods by solution-based method.

Keywords: ZnO, Nanorods, Sol–Gel, Formation Mechanism, Crystal Growth.

1. INTRODUCTION

Zinc oxide with the unique properties of wide band gap (3.3 eV), high exciton energy (60 meV), excellent thermal and mechanical stability is an important semiconductor material with significant value in both fundamental research and applications.¹ Recently, fabrication of ZnO nanostructures via solution-based approaches has drawn increasing research interest. Methods like sol–gel technique,^{2–4} chemical bath deposition (CBD),^{5,6} hydrothermal or solvothermal process,^{7–12} electrophoretic deposition etc.¹³ are promising candidates for industrialized preparation of ZnO nanomaterials with merits of low cost, large scale and high efficiency. Particularly, the fabrication of one-dimensional (1D) ZnO nanostructures (nanowires, nanorods and nanotubes) is paid extra attention due to their high application potential in solar cells,^{14,15} lasers,^{6,16} gas or biosensors,^{17,18} photodetectors¹⁹ and field effect transistors.²⁰

The mechanism of crystal formation in the solution can be generally described by the Ostwald ripening, which

suggests an ensemble of small crystalline nuclei in a supersaturated medium would selectively evolve into large particles at the expense of other small ones by the benefit of lower free energy.^{21,22} Such theory doesn't explain how the anisotropic growth takes place resulting 1D nanostructures instead of sphere like nanoparticles. Li et al. modified the conventional Periodic Bond Chain (PBC) theory and proposed an ideal growth mechanism. It considers the interface structure of oxide crystals as the stacking order of coordination polyhedrons whose favored orientation during the solution growth shapes the obtained crystals.²³ Their model suggests that the growth rate of ZnO (0001) face is faster than the (01-10) face which results in the hexagonal rod shape ZnO with the polar face (0001) and (000-1) at the two ends. Recently, another route "oriented attachment" is discovered for 1D ZnO nanostructure growth. Found by Pacholski et al. quasi spherical particles with the size of several nanometers can gradually aggregate with each other to form secondary particles driven by the gain of free lattice energy and free energy of polycondensation.²² The preferentially growth along the *c*-axis is speculated to be related to the wurtzite structure itself. In order to boost the 1D crystal growth,

*Author to whom correspondence should be addressed.

capping reagents or surfactants such as hexamethylenetetramine (HMT), sodium dodecyl sulfate (SDS) are used in the hydrothermal growth.^{24–26} The diameters and lengths of nanorods can be altered by changing the surfactants' concentration. However, their detailed effect during the growth is still under debate. O'Brien et al. suggested that HMT is a poor ligand for zinc. The primary role of HMT is to act as a PH buffer. It's a slow controlled supply of OH[−] and helps the formation of complex zinc(II) intermediates.^{5, 26} Imai et al. studied the growth condition for wurtzite ZnO in aqueous solution and concluded that a basic condition is favored by ZnO crystal growth in the aqueous.²⁷ Other experimental factors such as solvents, sol concentration are also investigated.^{28, 29}

The growth mechanism of 1D ZnO in solution is complex and the obtained nanocrystal morphology is very sensitive to various experiment parameters. In this paper, ZnO nanorods were fabricated on glass substrates via spin-coating aged sol–gel and annealing. The experimental setting is rather similar to what is used for the growth of traditional ZnO thin films.³ The sol is absent of HMT and not in a strong basic condition. The experiment could thus help to clarify the intrinsic factors that distinguish anisotropic growth from the uniform crystal growth. Evidence in transmission electron microscope (TEM) and photon correlation spectroscopy corroborated the nucleation process during sol aging and related the morphology change of the product with the aging time. In addition, ZnO nanorods were assembled on glass substrates without a process of keeping the substrate in the solution, which avoid the long time contact of sensitive substrates with solution.

2. EXPERIMENTAL DETAILS

2.1. Preparation of the Sol

Certain amount of zinc acetate dehydrate ($\text{Zn}(\text{CH}_3\text{COOH})_2 \cdot 2\text{H}_2\text{O}$, Analytic grade) and Monoethanolamine (MEA, Analytic grade) were added into 50 ml absolute ethanol to obtain 0.75 M sol, while the molar ratio of $\text{Zn}(\text{Ac})_2 \cdot 2\text{H}_2\text{O}$ and MEA are kept at 1. MEA here served as a stabilizer to promote the dissolution of $\text{Zn}(\text{Ac})_2$ in the ethanol. After stirred for one hour at a constant temperature of 60 °C, the resultant solution was clean and transparent.

The solution is then kept in closed flasks at room temperature to age for one day (one day solution, 1DS), one month (1MS), two months (2MS) and four months (4MS) before the coating process.

2.2. Synthesis of ZnO Nanostructured Film on Glass Substrate

The solution aged for certain time was spin coated on glasses substrates at 4000–5000 r/pm at room temperature. The sample was annealed in air ambient to obtain a

half-transparent white film on the glass. The anneal temperature was increased from room temperature to 550 °C at 4 °C/min rate and kept at 550 °C for 3 hours. In order to study the formation process, special samples are prepared with only a preheating at 60 °C for 30 min.

2.3. Characterization

The morphologies of the films and nanorods were characterized by scanning electron microscope (SEM) (Philips XL30FEG) and transmission electron microscope (TEM) (JEM-2010). To investigate the formation mechanism of nanorods, photon correlation spectroscopy (Zetasizer Nano S, Malvern Instruments Ltd.) was used to analyze the size distribution of small nanoparticles formed in the solution after aging process. The test was assisted by a centrifuge (8000, Shanghai Surgical instruments Factory) and details will be described below. The crystalline structures of the preheated film were characterized via X-ray diffraction spectroscopy (XRD) (Bruker AXS: D8 Discover with General Area Detector Diffraction System with X-ray radiation from Cu-K α , $\lambda = 1.5418 \text{ \AA}$). The Raman spectra and PL measurements were carried out with Jobin Yvon LabRAM HR 800UV micro-Raman system with the 325 nm He–Cd laser (for PL spectra) and 514 nm laser (for Raman Spectra) and an Andor DU420 classic CCD detector.

3. RESULTS AND DISCUSSION

3.1. Morphology Study

Figures 1(a), (b) and (c) show the SEM images of ZnO products obtained on the glass by spin-coating with 1MS, 2MS and 4MS respectively. Hexagonal nanorods embedded in ZnO films can be clearly seen on each image. Figure 1(f) gives the TEM image and SAED pattern of one single nanorod, which confirms the nanorods are ZnO wurtzite structure with growth direction [0001]. The nanorods are more productive on the 2MS and 4MS samples and the sizes of nanorods are bigger on the 4MS sample. In contrast, the sample spin-coated by 1DS resulted in a uniform thin film without any nanorods on it (Fig. 1(e)). Figure 1(d) is the magnified SEM images of selected ZnO nanorods found on 1MS, 2MS and 4MS samples. Some of the nanorods have their both ends exposed in the air (marked by white circles). Such phenomena suggest us that the nanorods embedded in the films are more likely to grow by a homogeneous nucleation rather than heterogeneously grow from the glass surface directly.

3.2. Formation Mechanism Investigation

The results above indicated that the sols kept at room temperature for different time yielded the different results while other experimental processes remain the same. It is

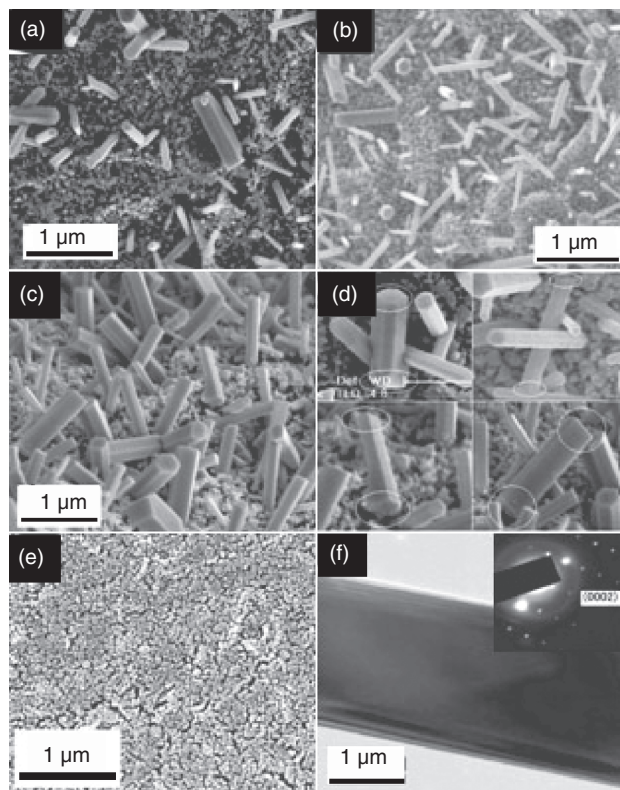


Fig. 1. Morphologies of ZnO nanorods obtained on glass substrates by sol–gel spin coating using (a) 1MS (one month aged sol), (b) 2MS and (c) 4MS; (d) the magnified SEM images of selected nanorods showing their two ends unburied; (e) uniform thin film without rod shape crystals prepared by fresh sol; (f) TEM image and SAED pattern of one obtained nanorod.

reasonable to speculate that the compositions of the sol must have changed during the aging process and it assisted the anisotropic growth of 1D nanorods. Illuminated by the results from Figure 1(d), we suspected that small ZnO crystalline particles might have already formed in the aged sol through slow homogenous nucleation. Similar phenomena are observed by Cao et al. where they studied ZnO nanorods growth in room temperature aged solution.³⁰

In order to confirm our speculation, photon correlation spectroscopy was used to test the size distribution of the possible ZnO particles. Before the testing, we first centrifuged the sol so that the speculated particles could be more concentrated. After the centrifuge, the sol observed by naked eye still remained clean and no clear precipitants or stratification was observed. This indicated that even if there are ZnO particles formed, the size of them should not be large. The sol located at the bottom part of the centrifuge tube was extracted for our testing. The results of 1MS and 2MS are shown in Figures 2(a), (b) respectively. The dispersant was set as ethanol with reflection index (RI) 1.361 and viscosity 1.17. The material RI was 2.008 for ZnO. The obtained polydispersity index (PDI) is 0.405 for 1MS and 0.842 for 2MS. The size distribution of each solution both have the peak centered around

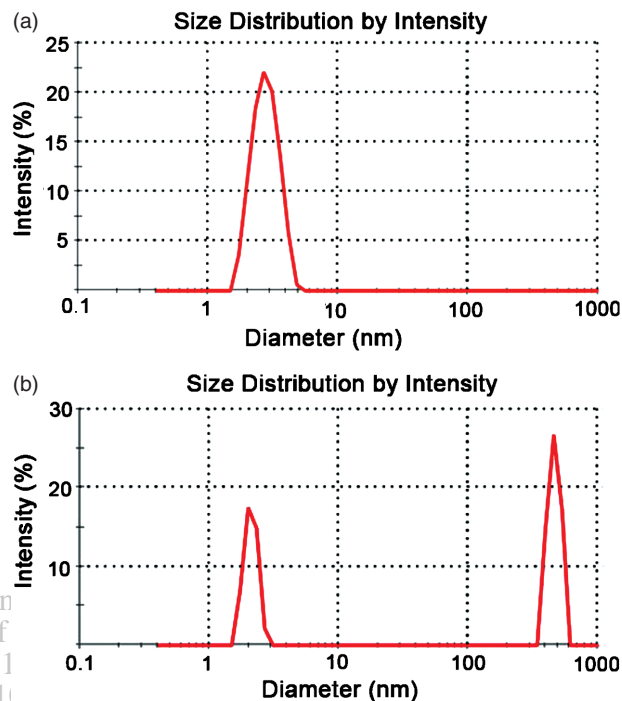


Fig. 2. Size distribution of nanoparticles formed in the (a) 1MS and (b) 2MS by photon correlation spectroscopy. The peak of 1MS sample is located at 2.83 nm and two peaks of 2MS sample are located at 2.11 nm and 464.1 nm.

2–3 nanometers (2.83 nm, 1MS and 2.11 nm, 2MS) with intensity 94.92% for 1MS and 40.6% for 2MS. This confirmed our speculation that small particles were formed during the aging process. Particularly for the 2MS, another peak centered at 464.1 nm (58.5% intensity) was detected. This suggested that large crystalline particles with size of hundred nanometers have formed and it was likely that small particles have the tendency to aggregate with each other and they together formed loosely-packed clusters which originated the peak. For the 4MS sample, the test results are found varied greatly each time. It is not able to give a credible result. This would be explained later with TEM results.

The solutions were further subjected to TEM analysis. Sample solutions were firstly centrifuged and the bottom part of the sol in the tubes was extracted. They were diluted by absolute ethanol (in case they dried to form a thick gel layer that conceal the desired contents from our observation) and was dropped onto the copper screen in tiny amount. Figures 3(a), (b) and (c) give the TEM images of the 1MS, 2MS and 4MS samples. Figures 3(d), (e) and (f) are the corresponding SAED pattern. In Figure 3(a), most part of the sol is clear without big clusters with only several small black spots to be found. In contrast, after 2 months aging, many aggregates with several hundred nanometers diameters began to exist in the sol (Fig. 3(b)). The results are in accordance with the particle size distribution diagram. Figures 3(d) and (e) are

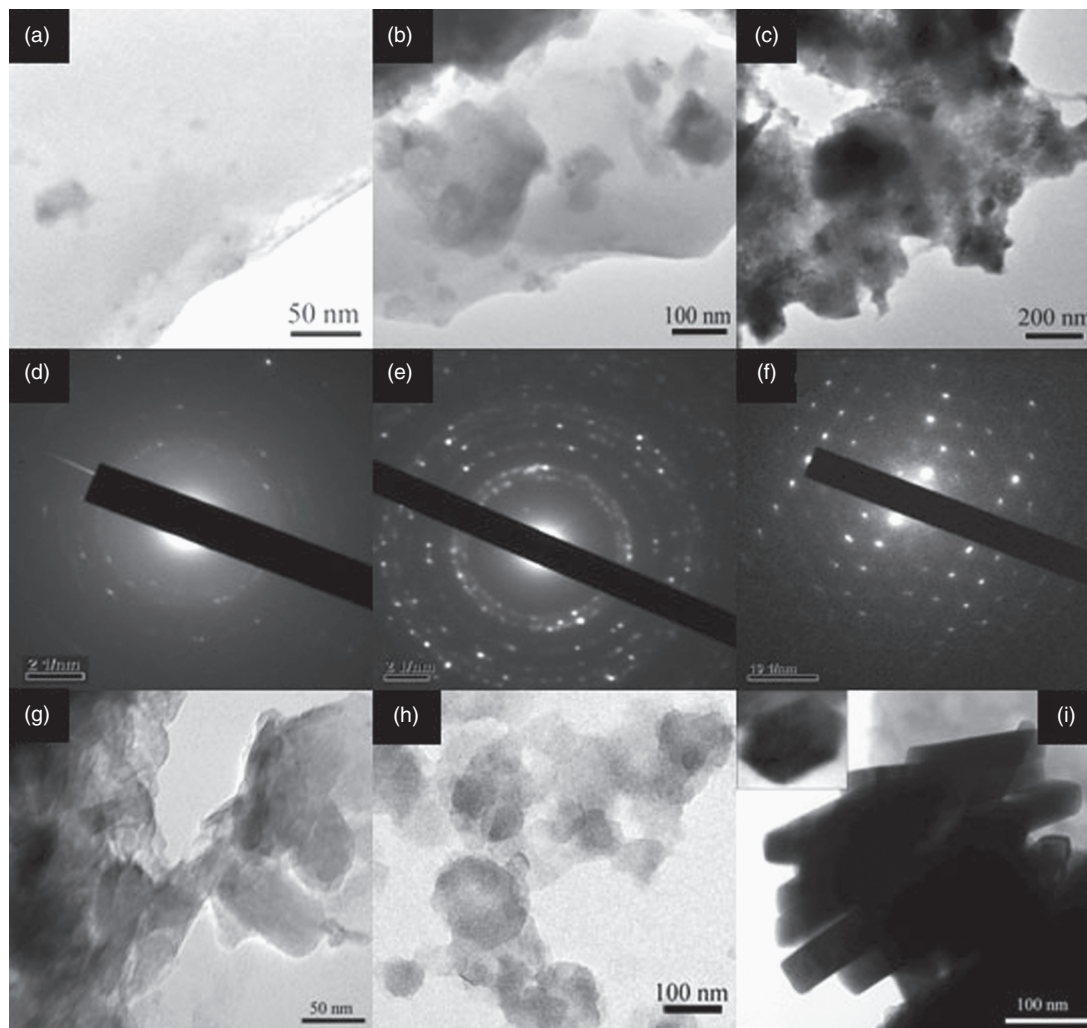


Fig. 3. TEM images showing the condition in (a) 1MS, (b) 2MS and (c) 4MS with the corresponding SAED pattern (d) 1MS, (e) 2MS and (f) 4MS; TEM images of the contents obtained on glass substrates after a pre-heating process for (g) 1MS, (h) 2MS and (i) 4MS. The inset of Figure 3(i) shows a hexagonal shape face of one nanoparticle.

the corresponding SAED pattern. They are the evidence of crystalline particles formed in the sol. Figure 3(e)'s diffraction rings were interpreted into crystal faces with interplanar distances (from inside to out) of 2.6 Å, 2.3 Å, 1.6 Å, 1.4 Å which can be indexed to (002), (101), (102), (103) faces from hexagonal wurtzite structure of ZnO. It confirmed that the crystalline nanoparticles were zinc oxide. Figure 3(c) shows the aggregation tendency in the aging process. The 4MS obviously were denser with many bigger clusters (dark spots) formed. Its SAED pattern directly proved the existence of single crystalline nanocrystals. Such condition explained why the photon correlation spectroscopy of 4MS varied greatly each time. The solution was actually close to being an unstable solution system. Though the 4MS was clean by naked eye observation, there were actually more particles or clusters presenting in the solution. The viscosity would be higher and the solution might lose its high mobility, which caused the uneven distribution of precipitated contents. This would

obscure the photon correlation test and lead to the failure of the test. All these results coincide with our speculation and indicate the fact that during the aging process, small crystalline ZnO particles begin to form by homogenous nucleation into the size of several nanometers. These small nanoparticles have the tendency to aggregate with each other to form larger clusters. It prepares and influences the further crystalline process during the annealing.

3.3. Anneal Effect

Special samples were then prepared by spin-coating 1MS, 2MS and 4MS on the glass substrate followed by a 60 °C, 30 min heating process. Figures 3(g, h and i) are the TEM images of the obtained products in the coating layer. The further aggregation and crystal growth were taking place during the heating. Figure 3(h) gives bigger particles with more clear edges and angles. Where there are no nanorods

found on the samples prepared by 1MS and 2MS pre-heating samples, Figure 3(i) was nanorods formed already on the 4MS sample. The inset of Figure 3(i) clearly demonstrated a hexagonal end of the nanoparticles. The difference of aging time gave the different condition in the sol and caused the next growing step with divergent results.

The pre-heated 4MS sample was then subjected into XRD analysis to clarify the substance of the nanocrystal. Figure 4(a) is the XRD diffraction pattern with peaks matches with wurtzite ZnO (100), (002), (101) and (102) faces. The result confirmed that ZnO products had already formed in pre-heated layer. The broad peak centered at 60 degree didn't match (110) or (103) faces. According to PDF#-740094, this peak could be assigned to an imposition of signals from Zn(OH)₂ faces. This is reasonable as Zinc hydroxyl or Zn(OH)_x complexes are found during the sol-gel process and the sample hadn't undergone the entire annealing process.^{31,32} The more interesting results are the small angle area diffraction. Figure 4(b) is the detected diffraction pattern. The spectrum is shown in Figure 4(c). A series peak with similar interval was observed. Suspecting that they came from the same indexed faces, we fit it

with the diffraction formula where λ equals to 1.5418 Å:

$$2d \sin(\theta) = n\lambda \quad (1)$$

The experimental data fit well with the linear line. The interplanar distance d is found to be 2.351 nm. Such small angel XRD pattern being detected indicated that the primitive nucleated nanoparticles began to stack into ordered layered Zinc complexes during the pre-heating. The result could also be linked with the results of the photon correlation spectroscopy where both 1MS and 2MS had size distribution peaks at 2–3 nm. Though photon correlation spectroscopy test of 4MS sample failed to give a credible result, it could be speculated on the tendency of the 1MS and 2MS samples' result and the 4MS sample's XRD spectroscopy that while the aggregation of nanoparticles kept evolving into secondary clusters during the aging, the primitive nucleated particles held the size of 2–3 nanometers.

Figure 5 shows the Raman and PL spectra for samples prepared by 1MS, 2MS and 4MS. Figures 5(a) and (b) are spin-coated samples treated only with pre-heating process. There are broad peaks at 575 cm⁻¹ in Raman spectra

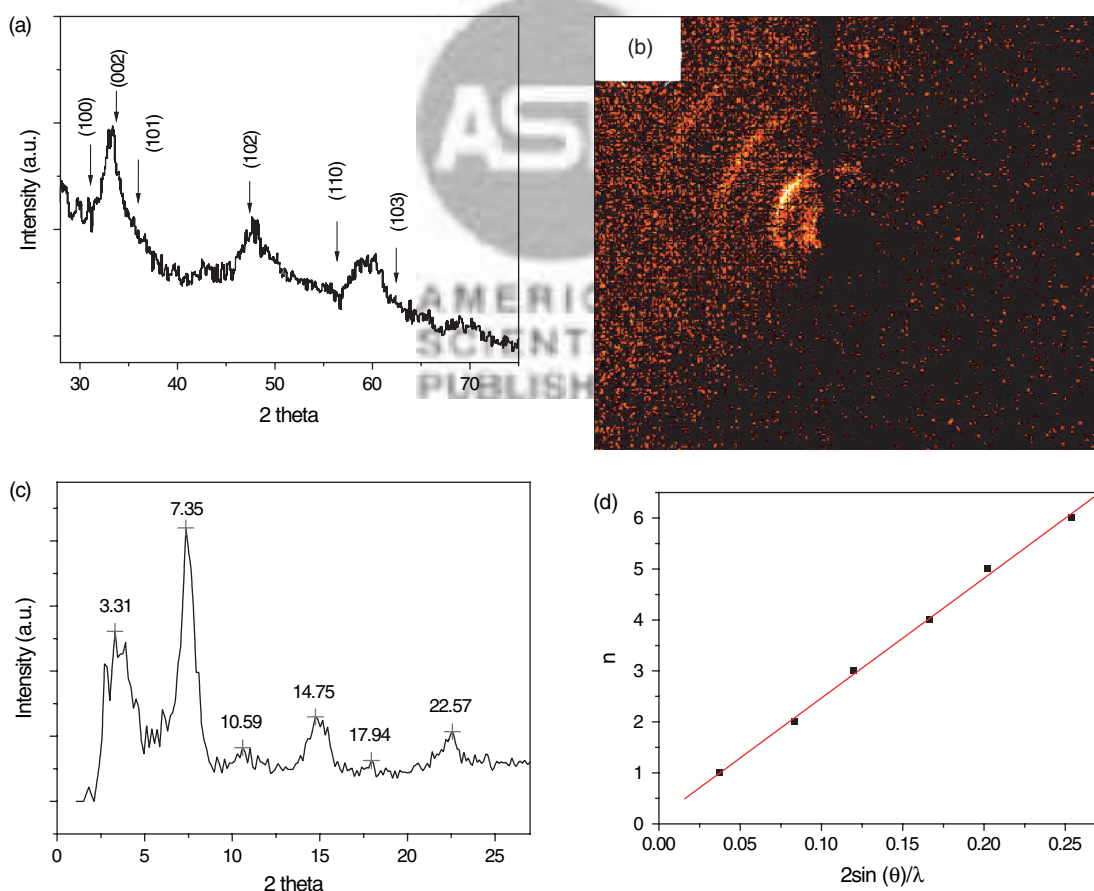


Fig. 4. (a) X-ray diffraction spectrum of ZnO products by spin-coating with 4MS and preheated at 60 °C for 30 min; (b) photo images of diffraction signals; (c) small angle range XRD showing 5 peaks with nearly the same intervals; (d) linear fit of the 5 small angel peaks data by the formula: $2d \sin(\theta) = n\lambda$ ($\lambda = 1.5418$ Å).

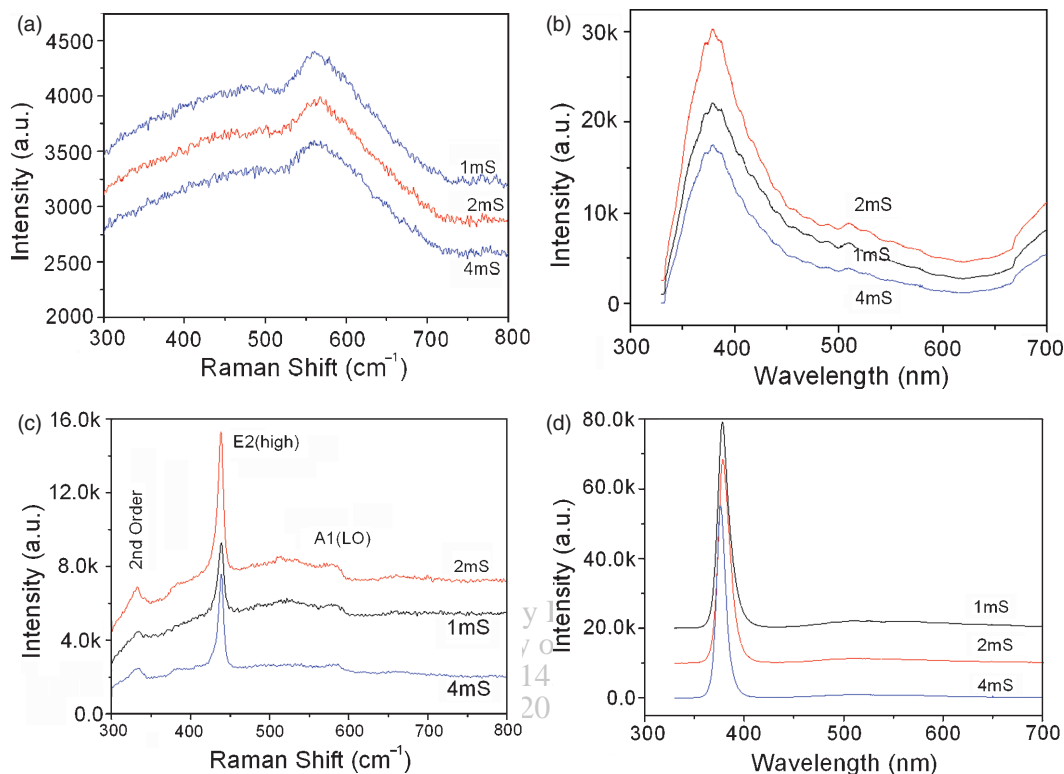


Fig. 5. (a) Raman and (b) PL spectra for ZnO nanorods samples with pre-heating; (c) Raman and (b) PL spectra for ZnO nanorods samples prepared by the entire annealing process.

(Fig. 5(a)) assigned to ZnO A1(LO) mode and peaks at 380 nm in PL spectra (Fig. 5(b)) originated by near band emission.^{33,34} After annealing, Figure 5(c) shows the strong Raman peak at 438 cm^{-1} belong to E2(high) mode with weak signal at 580 cm^{-1} (A1(LO)) and 331 cm^{-1} (second order Raman spectrum) which confirmed high quality crystalline ZnO were obtained after annealing.³³ The PL spectra corroborated this by demonstrating strong UV emission with weak green emission originated from impurities.³⁴ The spectra comparison between annealed and pre-heated samples suggests that the post annealing process prepare the final formation of ZnO crystals on the substrates.

Based on all the results above, our proposed formation mechanism are summarized in Figure 6. Firstly, the fresh sol is prepared (Fig. 6(a)). After aging, small crystalline nanoparticles nucleated and long term aging would yield big aggregation (Fig. 6(d)) just as the result of TEM study suggested (Figs. 3(a–c)). When the sol is spin coated on the glass substrate and undergoes anneal, the solvent begins to evaporate starting at relative low temperature. The secondary nucleation and growth of crystals occurs in the coated layer through competition. The difference here is that for the fresh sol, the nucleation is evenly distributed on the substrate. Because zinc complexes formed would soon lose their mobility during anneal, there is low chance to form large crystals (Fig. 6(b)). After post

annealing, the sample prepared by fresh sol would then grow into uniform thin films (Fig. 6(c)). For the aged sol, the already nucleated nanoparticles would become the nucleation center attracting other molecules around in a short time and grow into bigger sizes (Fig. 6(e)). The age of sol is therefore essential because the primitive nucleation and aggregation takes place in the slow aging process which provides the nucleation centers as well as guarantees sufficient time for the secondary growth of larger and

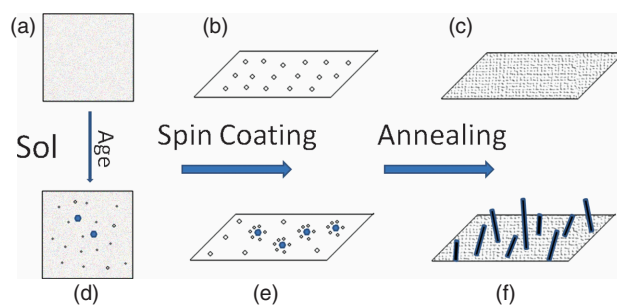


Fig. 6. Schematic images describe the formation mechanism of ZnO nanorods in the spin-coating process. (a) The fresh sol is transparent with no crystalline particles. (b) When fresh sol is spin-coated on the substrate, the nucleation will evenly occur and (c) form a uniform thin film. (d) After room temperature aging, small particles formed in the sol and have the tendency to aggregate with each other. (e) When aged sol is spin-coated on the substrate, the already existed particle will serve as the nucleation center and (f) lead to the form of nanorods.

anisotropic ZnO during the rapid process of solvents evaporation and decomposition. The form of nanorods is due to the nature of wurtzite ZnO itself. The MEA here may played a similar role as HMT to assist the anisotropic growth along [0002] direction. We speculated is that MEA firstly provides OH^- and helps to form zinc complexes $\text{Zn}(\text{Ac})_x(\text{OH})_{4-x}^{2-x}$ acting as growth units.⁵ Affect by the intrinsic polar of wurtzite ZnO, the growth units prefer to bonding to the ZnO (002) faces and transform into ZnO by dehydration and decomposition. This is similar to the formation mechanism proposed by Li et al.²³ The MEA might also coordinate to the existed ZnO nanoparticles, hindering the growth of lateral faces.²⁹ The reason why large single crystalline ZnO nanorods didn't form during aging process already is that in such room temperature, non-basic solution, there isn't a thermodynamically favored condition for large wurtzite ZnO crystal growth.

4. CONCLUSION

In summary, ZnO nanorods were successfully synthesized on glass substrate via spin coating aged sol–gel process with non-basic zinc acetate solution using ethanol as the solvents. The formation of ZnO nanorods is through two separated steps: the nucleation and aggregation of small nanoparticles in the aged sol and the anisotropic growth of nanorods during annealing. The formation of small crystalline particles is corroborated by photon correlation spectroscopy, TEM study and SAED pattern. The heating effect is then investigated by XRD, TEM, PL and Raman Spectroscopy with consistence results demonstrating that the condition in the aged sol would affect next step crystal growth. This approach is simple and the substrates are not required to be kept in the stirring solution for a long time. It provides an alternative way to fabricate ZnO nanorods based devices.

Acknowledgment: This work was supported by the Natural Science Foundation of China (grant NO. 50572064, 10874115, 10734020), National Minister of Education Program of IRT0524 and Shanghai Key Basic Research Project of 08JC1411000.

References and Notes

1. J. G. Lu, P. Chang, and Z. Fan, *Mater. Sci. Eng. R* 52, 49 (2006).
2. M. Ohyama, H. Kozuka, and T. Yoko, *Thin Solid Films* 306, 78 (1997).
3. H. Li, J. Wang, H. Liu, H. Zhang, and X. Li, *J. Cryst. Growth* 275, e934 (2005).

4. K. Han, Z. Zhao, Z. Xiang, C. Wang, J. Zhang, and B. Yang, *Mater. Lett.* 61, 363 (2007).
5. K. Govender, D. S. Boyle, P. B. Kenway, and P. O'Brien, *J. Mater. Chem.* 14, 2575 (2004).
6. K. Govender, D. S. Boyle, P. O'Brien, D. Binks, D. West, and D. Coleman, *Adv. Mater.* 14, 1221 (2002).
7. L. Vayssieres, *Adv. Mater.* 15, 464 (2003).
8. Z. R. Tian, J. A. Voigt, J. Liu, B. Mckenzie, M. J. Mcdermott, M. A. Rodrigues, H. Konoshi, and H. Xu, *Nat. Mater.* 2, 821 (2003).
9. B. Liu and H. C. Zeng, *J. Am. Chem. Soc.* 125, 4430 (2003).
10. S. K. N. Ayudhya, P. Tonto, O. Mekasuwandumrong, V. Pavarajarn, and P. Praserttham, *Cryst. Growth Des.* 6, 2446 (2006).
11. O. Mekasuwandumrong, P. Tonto, S. Phatanasri, V. Pavarajarn, and P. Praserttham, *Ceram. Int.* 34, 57 (2008).
12. S. Kar, A. Dev, and S. Chaudhuri, *J. Phys. Chem. B* 110, 17848 (2006).
13. Y. C. Wang, I. C. Leu, and M. H. Hon, *J. Cryst. Growth* 237–239, 564 (2002).
14. M. Law, L. E. Greene, J. C. Johnson, R. Saykally, and P. Yan, *Nat. Mater.* 4, 455 (2005).
15. J. B. Baxter, A. M. Walker, K. Van Ommering, and E. S. Aydil, *Nanotechnology* 17, S304 (2006).
16. M. H. Huang, S. Mao, H. Feick, H. Yan, Y. Wu, H. Kind, E. Weber, R. Russo, and P. Yang, *Science* 292, 897 (2001).
17. J. X. Wang, X. W. Sun, Y. Yang, H. Huang, Y. C. Lee, O. K. Tan, and L. Vayssieres, *Nanotechnology* 17, 4995 (2006).
18. A. Dorfman, N. Kumar, and J. Hahm, *Adv. Mater.* 18, 2685 (2006).
19. Y. Lin, C. Chen, W. Yen, W. Su, C. Ku, and J. Wu, *Appl. Phys. Lett.* 92, 233301 (2008).
20. P. Chang, Z. Fan, C. Chien, D. Stichtenoth, C. Ronning, and J. G. Lu, *Appl. Phys. Lett.* 89, 133113 (2006).
21. L. Spanhel and M. A. Anderson, *J. Am. Chem. Soc.* 113, 2826 (1991).
22. C. Pacholski, A. Kornowski, and H. Weller, *Angew. Chem. Int. Ed.* 41, 1188 (2002).
23. W. Li., E. Shi, W. Zhong, and Z. Yin, *J. Cryst. Growth* 203, 186 (1999).
24. A. Dev, S. K. Panda, S. Kar, S. Chakrabarti, and S. Chaudhuri, *J. Phys. Chem. B* 110, 14266 (2006).
25. L. Vayssieres, K. Keis, S. Lindquist, and A. Hagfeldt, *J. Phys. Chem. B* 105, 3350 (2001).
26. L. E. Greene, B. D. Yuhas, M. Law, D. Zitoun, and P. Yang, *Inorg. Chem.* 45, 7535 (2006).
27. S. Yamabi and H. Imai, *J. Mater. Chem.* 12, 3773 (2002).
28. T. Andelman, Y. Gong, M. Polking, M. Yin, I. Kuskovsky, G. Neumark, and S. O'Brien, *J. Phys. Chem. B* 109, 14314 (2005).
29. H. Bahadur, A. K. Srivastava, A. K. Rashmi, and S. Chandra, *IEEE Sensors J.* 8, 831 (2008).
30. H. L. Cao, X. F. Qian, Q. Gong, W. M. Du, X. D. Ma, and Z. K. Zhu, *Nanotechnology* 17, 3632 (2006).
31. E. Hosono, S. Fujihara, T. Kimura, and H. Imai, *J. Sol–Gel Sci. Technol.* 29, 71 (2004).
32. S. Bandyopadhyay, G. K. Paul, R. Roy, S. K. Sen, and S. Sen, *Mater. Chem. Phys.* 74, 83 (2002).
33. T. C. Damen, S. P. S. Porto, and B. Tell, *Phys. Rev.* 142, 570 (1966).
34. K. Vanheusden, W. L. Warren, C. H. Seager, D. R. Tallant, J. A. Voigt, and B. E. Gnade, *J. Appl. Phys.* 79, 7983 (1996).

Received: 12 November 2008. Accepted: 13 March 2009.